Journal of Computational and Nonlinear Dynamics Journal

Copy of e-mail Notification

Journal of Computational and Nonlinear Dynamics Published by ASME

Dear Author,

YOUR PAGE PROOF IS AVAILABLE IN PDF FORMAT; please refer to this URL address
http://115.111.50.156/jw/AuthorProofLogin.aspx?pwd=f8e2e19d935f

Login: your e-mail address
Password: f8e2e19d935f

The site contains 1 file. You will need to have Adobe Acrobat Reader software to read these files. This is free software and is available for user downloading at http://www.adobe.com/products/acrobat/readstep.html.

This file contains:

Adobe Acrobat Users - NOTES tool sheet, a copy of your page proofs for your article

Please read the page proofs carefully and:
1) indicate changes or corrections using e-annotation;
2) answer all queries;
3) proofread any tables and equations carefully;
4) check that any special characters have translated correctly.
5) upload annotated pdf file to the URL address above.

Special Notes:

Your Login and Password are valid for a limited time. Your prompt attention to and return of page proofs will help expedite publication of your work. Thank you for your cooperation.

If you have any questions regarding your article, please contact me. PLEASE ALWAYS INCLUDE YOUR ARTICLE NO. (CND-11-1183) WITH ALL CORRESPONDENCE.

This e-proof is to be used only for the purpose of returning corrections to the publisher.

Sincerely,

Isabel Castillo, Journal Production Manager, E-mail: Isabel.Castillo@cenveo.com

AUTHOR QUERY FORM

ASME SETTING THE STANDARD	Journal: J. Comput. Nonlinear Dynam. Article Number: CND-11-1183	**Please provide your responses and any corrections by annotating this PDF and uploading it to ASME's eProof website as detailed in the Welcome email.**

Dear Author,

Below are the queries associated with your article; please answer all of these queries before sending the proof back to Cenveo. Production and publication of your paper will continue after you return corrections or respond that there are no additional corrections.

Location in article	Query / Remark: click on the Q link to navigate to the appropriate spot in the proof. There, insert your comments as a PDF annotation.
AQ1	Please confirm that the range should read "25–50" instead of "[25 50]" in the sentence beginning "The values of the and parameters have to assure the right balance."
AQ2	Please confirm that is meant to appear twice in the sentence beginning "where the natural abscissas of the contact points."
AQ3	Please confirm the revision of the sentence beginning "In fact, the necessity of acceptable computational time" retains its intended meaning.
AQ4	Please clarify the sentence beginning "The last step consists of the update of the old profiles."
AQ5	Please confirm that DM061, DM068, and DM082 are correct in the sentence beginning "The experimental data provided by Trenitalia and RFI."
AQ6	Please confirm that MD061 is correct and should not be DM061 in the sentence beginning "As can be seen by example in Table 4."
AQ7	Please confirm that MD061, MD068, and MD082 are correct in the sentence beginning "The arithmetic mean on the three vehicle MD061, MD068, and MD082."
AQ8	Please confirm that "Engg." is the intended title abbreviation in the Acknowledgments section.
AQ9	Please confirm the correct publication year for Ref. 12 and delete the one that is incorrect. If 2001 is correct, please move this year to the appropriate location in the reference.
AQ10	Please provide DOI for the ref. 7.

Thank you for your assistance.

Development of a Model for the Prediction of Wheel and Rail Wear in the Railway Field

M. Ignesti
e-mail: ignesti@mapp1.de.unifi.it

L. Marini
e-mail: marini@mapp1.de.unifi.it

E. Meli
e-mail: meli@mapp1.de.unifi.it

A. Rindi
e-mail: rindi@mapp1.de.unifi.it

Department of Energy Engineering,
University of Florence,
50139 Firenze, Italy

The wear prediction at the wheel-rail interface is a fundamental problem in the railway field, mainly correlated to the planning of maintenance interventions, vehicle stability, and the possibility of researching strategies for the design of optimal wheel and rail profiles from the wear point of view. The authors in this work present a model specifically developed for the evaluation of the wheel and rail wear and of the wheel and rail profiles evolution. The model layout is made up of two mutually interactive parts: a vehicle model for the dynamical analysis and a model for the wear estimation. The first one is a 3D multibody model of a railway vehicle where the wheel-rail interaction is implemented in a C/C++ user routine. Particularly, the research of the contact points between wheel and rail is based on an innovative algorithm developed by authors in previous works, while normal and tangential forces in the contact patches are calculated according to the Hertz and Kalker's global theory, respectively. The wear model is mainly based on experimental relationships found in literature between the removed material by wear and the energy dissipated by friction at the contact. It starts from the outputs of the dynamical simulations (position of contact points, contact forces, and global creepages) and calculates the pressures inside the contact patches through a local contact model; then, the material removed by wear is evaluated and the worn profiles of wheel and rail are obtained. In order to reproduce the wear evolution, the overall mileage traveled by the vehicle is divided into discrete steps, within which the wheel and rail profiles are constant; after carrying out the dynamical simulations relative to one step, the profiles are updated by means of the wear model. Therefore, the two models work alternately until completing the whole mileage. Moreover, the different time scales characterizing the wheel and rail wear evolutions require the development of a suitable strategy for the profile update; the strategy proposed by the authors is based both on the total distance traveled by the vehicle and on the total tonnage burden on the track. The entire model has been developed and validated in collaboration with Trenitalia S.p.A. and Rete Ferroviaria Italiana (RFI), which have provided the technical documentation and the experimental results relating to some tests performed with the vehicle DMU Aln 501 Minuetto on the Aosta-Pre Saint Didier line. [DOI: 10.1115/1.4006732]

Keywords: multibody modeling, wheel-rail contact, wheel-rail wear

1 Introduction

The wear at the wheel-rail interface is an important problem in the railway field. The evolution of the profile shape due to wear has a deep effect on the vehicle dynamics and on its running stability, leading to performance variations both in negotiating curves and in a straight track. Therefore, the original profiles have to be periodically re-established by means of turning; particularly, from a safety viewpoint, the arising of a contact geometry, which may compromise the vehicle stability or increase the derailment risk, has to be avoided. As a matter of fact, vehicle instability could appear even at low speeds, in the case of high equivalent conicity in the wheel-rail coupling, whereas the derailment may be facilitated by low flange contact angles. Moreover, the planning and optimization of the maintenance intervals leads also to many advantages in terms of economic costs mainly correlated to the increase of the wheel's lifetime.

A reliable wear model can also be used to optimize the original profiles of wheel and rail in order to obtain a more uniform wear. In this way, the overall amount of removed material can be reduced, so as to increase the mean time between two maintenance intervals, and, at the same time, the dynamical performance of the wheel-rail pair can be kept approximately constant in the time. To this aim, Trenitalia has shown interest in developing new optimized wheel profiles, so to reduce the economic impact of management and maintenance of the railway vehicles.

It is important to underline that one of the most critical aspects in the development of a wear model is the availability of experimental results, since the collection of the data requires some months with relevant economic cost. In addition, for a correct interpretation of the data, they must be opportunely stratified to correlate the influent factors (vehicles characteristics, tracks, rail conditions, etc.) to the wear evolution. If online experimental measurement cannot be carried out, the problem could be overcome using tools provided by software [1,2] or carrying out experimental proofs on a scaled test rig [3].

In this work, the authors will present a procedure to estimate the evolution of the wheel and rail profile due to wear based on a model that combines multibody and wear modeling. More specifically, the general layout of the model consists of two parts mutually interactive: the vehicle model (multibody model and 3D global contact model) and the wear model (local contact model,

Contributed by the Design Engineering Division of ASME for publication in the Journal of Computational and Nonlinear Dynamics. Manuscript received October 26, 2011; final manuscript received December 21, 2011; published online xx xx, xxxx. Assoc. Editor: Tae-Won Park.

wear evaluation, and profiles update). The multibody model, implemented in the SIMPACK environment, accurately reproduces the dynamics of the vehicle, taking into account all the significant degrees of freedom. The 3D global contact model, implemented in C/C++ environment and developed by the authors in previous works [4,5], detects the wheel-rail contact points by means of an innovative algorithm based on a fully 3D semianalytic procedures and then, for each contact point, calculates the contact forces through Hertz's and Kalker's global theory [6,7]. Thanks to the numerical efficiency of the new contact model, the two models interact directly online during the simulation of the vehicle dynamics. As regards the wear estimation, the local contact model (FASTSIM algorithm) uses the outputs of the multibody simulations (contact points, contact forces, and global creepages) to calculate the contact pressures and the local creepages inside the contact patch, while the wear model, thanks to these quantities, evaluates the total amount of removed material due to wear and its distribution along the wheel and rail profiles. The removal of the material is carried out considering the three-dimensional structure of the contact bodies and the different time scales characterizing the wear evolution on wheel and rail. The whole procedure for the wear estimation is implemented in a MATLAB environment.

In this work, the entire model has been validated by means of the experimental data provided by Trenitalia S.p.A. and RFI; the data concern the Aosta-Pre Saint Didier railway line and the vehicle ALSTOM *DMU Aln 501 Minuetto*, which, in this scenery, exhibits serious problems in terms of wear.

2 Layout of the Model

The general architecture of the whole model is shown in the block diagram in Fig. 1; it includes two main parts that work alternatively during each step.

The *vehicle model* represents the part which is responsible for the dynamical simulation, and it is made up of the multibody model and of the global contact model; the two subsystems interact online during the simulations, creating a loop and reproducing the vehicle dynamics. The *wear model*, instead, is made up of three sub-parts: the local contact model, the wear evaluation, and the profile-updating procedure. In more detail, the multibody model exchanges data continuously at each time simulation step with the global contact model [4,5], passing the wheelset kinematic variables (wheelset position and orientation and their derivatives) and receiving the positions of the contact points, the wheel-rail contact forces, and the global creepages.

The main inputs of the vehicle model are the railway track and the multibody model of the considered vehicle; in this research activity, according to the specifications required by Trenitalia and considering the complexity and the length of the considered railway track, a statistical approach is necessary to achieve general significant results in a reasonable time. For these reasons, the entire Aosta-Pre Saint Didier line has been substituted with an equivalent set of different curved tracks, classified by radius, superelevation, and traveling speed, which has been built consulting a detailed track database provided by Rete Ferroviaria Italiana. Therefore, simulations have not been performed on the real railway line, but they have been carried out on an equivalent representation of this railway net, derived by means of statistical methods.

Once the multibody simulations are completed, the local contact model (based on the FASTSIM algorithm [6]) evaluates, starting from the global contact variables, the contact pressures and the local creepages inside each detected contact patch (and consequently divides it into adhesion area and creep area). Then, the distribution of removed material (hypothesizing the contact in dry conditions as required by Trenitalia and RFI) is calculated both on the wheel and on the rail surface only within the creep area using an experimental law between the removed material by wear and the energy dissipated by friction at the contact interface [3,8]. Finally, the wheel and the rail profiles are updated through suitable numerical procedures and represent the outputs of one discrete step of the whole model loop.

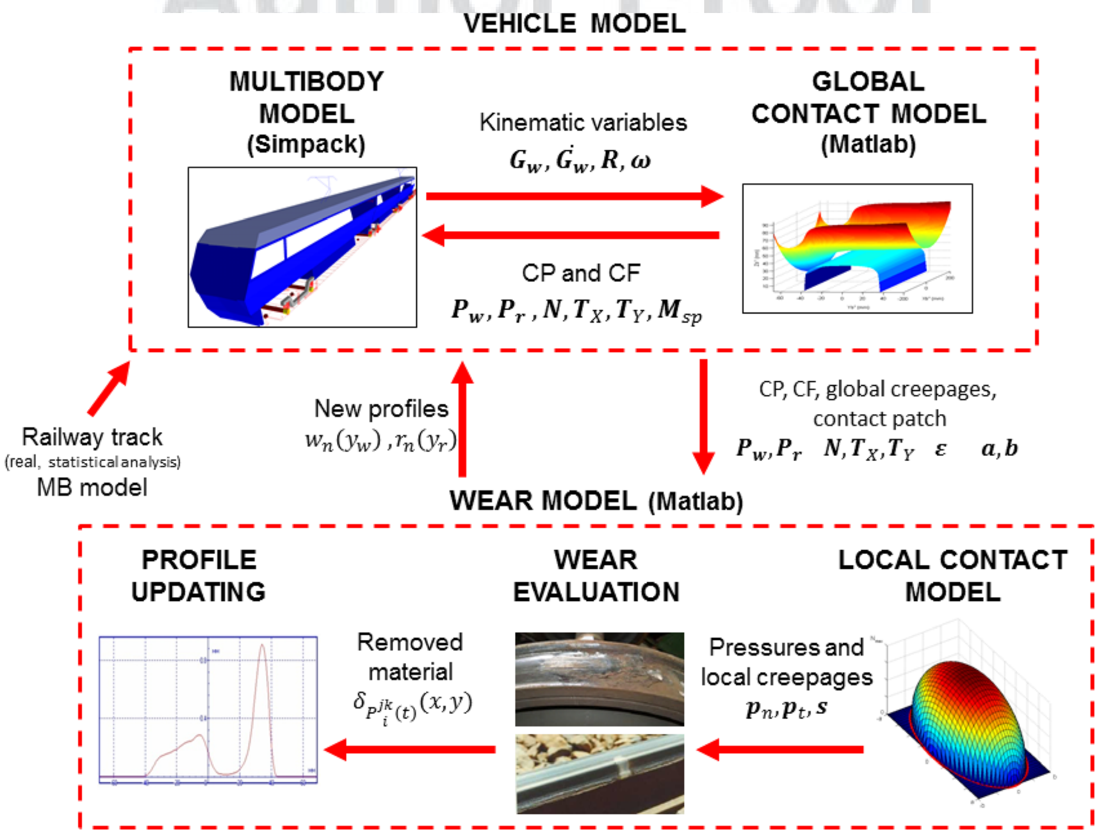

Fig. 1 General architecture of the model

The evolution of the wheel and rail profiles is therefore treated with a discrete approach. The entire mileage to be simulated is divided in a few spatial steps, within which the profiles are considered constant during the dynamical simulations; the results of the wear model, at the end of the current step, allow the update of the profiles for the next step of the procedure. The step length depends on the total distance to be covered and it is one of most important aspects of the entire numerical procedure, because it directly affects the precision. In fact, the smaller the step is, the higher the accuracy and the overall computation time are; hence, the choice has to be a compromise between these aspects. Moreover, from a numerical point of view, the step length can be chosen either constant during the overall distance or variable (introducing, for example, a threshold on the maximum of removed material); nevertheless, since the wear progress is almost linear with respect to the traveled distance, the constant step length turns out to be a quite suitable choice for this kind of problem, providing comparable results in terms of accuracy and better performance in terms of numerical efficiency. Finally, the discrete strategy has to consider the difference of time scale between the wheel and rail wear evolution rate (as will be clarified in the following), and from this point of view, the following considerations are valid:

- The wheel wear depends directly on the distance traveled by the vehicle; thus, the total traveled mileage, km_{tot}, has been subdivided in constant steps of length equal to km_{step}
- The depth of the rail wear instead does not depend on the distance traveled by vehicle, but on the number of vehicles moving on the track. Therefore, a different approach for evaluating the discrete step for the rail, based on the total tonnage burden on the track, M_{tot}, is needed. Dividing the total tonnage, M_{tot}, by the vehicle mass, M_v, the corresponding vehicle number, N_{tot}, has been calculated; then, N_{tot} has been subdivided in constant steps equal to N_{step}.

3 The Vehicle Model

In this section, a brief description of the vehicle model, made up of the multibody model and the global contact model, is given.

3.1 The Multibody Model. The *DMU Aln 501 Minuetto* has been chosen as the benchmark vehicle for this research; the physical and geometrical characteristics of the vehicle can be found in literature [9]. It is made up of three coaches and four bogies with two wheelsets; the external bogies are motorized, whereas the two intermediate trailer bogies are of Jacobs type, shared between two coaches. The multibody model has been realized in the SIMPACK environment (see Fig. 2) and consists of 31 rigid bodies: 3 coaches, 4 bogies, 8 wheelsets, and 16 axleboxes. The most significant inertial properties of the model bodies are summarized in Table 1.

The rigid bodies are connected by means of appropriate elastic and damping elements; particularly, the vehicle, as in the most part of passenger trains, is equipped with two suspension stages. The primary suspensions link the axlebox to the bogies (see Fig. 3) and comprise two springs and two vertical dampers, while the secondary suspensions connect the bogies to the coaches (see Fig. 4) and comprise the following elements:

- two air springs
- six dampers (lateral, vertical, and anti-yaw dampers)
- one traction rod
- the roll bar (not visible in the figure)
- two lateral bumpstops

Both the stages of suspensions have been modeled by means of three-dimensional viscoelastic force elements, taking into account all the mechanical non-linearities (bumpstop clearance, dampers, and rod behavior). The main linear characteristics of the suspensions are shown in Table 2.

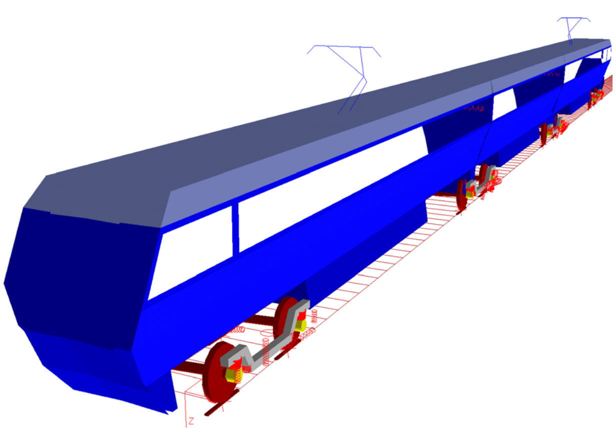

Fig. 2 Global view of the multibody model

Table 1 Inertia properties of the multibody model

MBS body	Mass (kg)	Roll inertia (kg m^2)	Pitch inertia (kg m^2)	Yaw inertia (kg m^2)
External coach	31 568	66 700	764 000	743 000
Internal coach	14 496	30 600	245 000	236 000
Bogie	3306	1578	2772	4200
Wheelset	2091	1073	120	1073

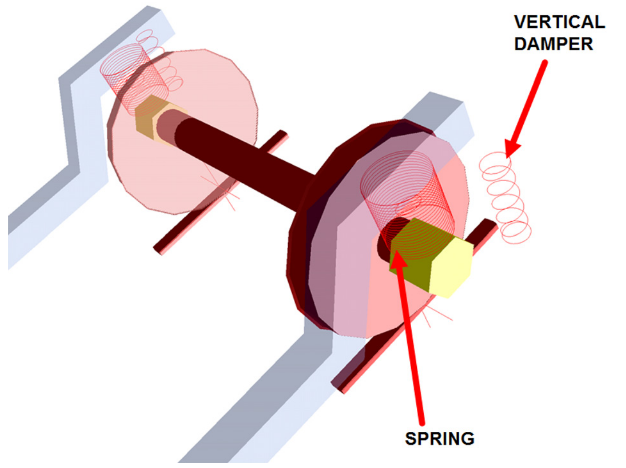

Fig. 3 Primary suspensions

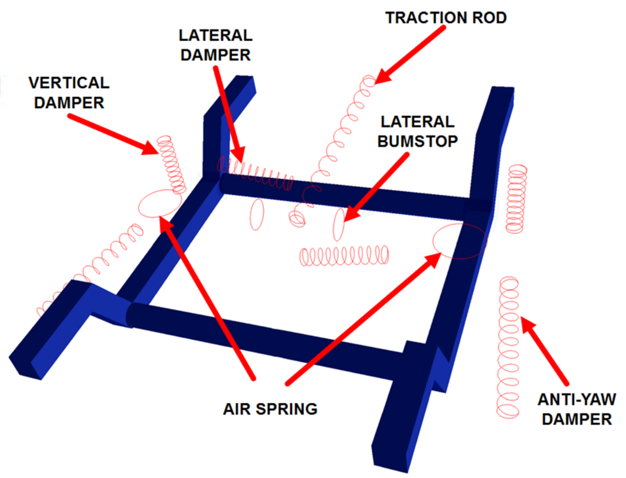

Fig. 4 Bogie and secondary suspensions

Table 2 Main linear stiffness properties of the suspensions

MBS element	Longitudinal stiffness (N/m)	Lateral stiffness (N/m)	Vertical stiffness (N/m)	Roll stiffness (Nm/rad)	Pitch stiffness (Nm/rad)	Yaw stiffness (Nm/rad)
Primary suspension spring	1 259 600	1 259 600	901 100	10 800	10 800	1000
Secondary suspension air spring	120 000	120 000	398 000	—	—	—
Secondary suspension roll bar	—	—	—	2 600 000	—	—

3.2 The Global Contact Model. Dynamic simulations of railway vehicles need a reliable and efficient method to evaluate the contact points at the wheel-rail interface, because their position has a considerable influence both on the direction and on the magnitude of the contact forces. In this work, a specific contact model has been considered instead of that implemented in SIMPACK in order to achieve better reliability and accuracy. The proposed contact model is divided in two parts: in the first one, the contact points are detected by means of an innovative algorithm developed by the authors in previous works [4,5], while in the second one, the global contact forces acting at the wheel-rail interface are evaluated by means of Hertz's and Kalker's global theories [6]. The new model is based on a semianalytic approach that guarantees the following features:

- generic wheel and rail profiles can be implemented
- fully 3D handling of the contact problem, with all degrees of freedom between wheel and rail taken into account
- no simplifying hypotheses on the problem geometry and kinematics
- multiple points of contact are allowed, with no bounds to their overall number
- high numerical efficiency, which allows the online implementation directly within the multibody models, without look-up tables; numerical performance better than those obtainable with commercial software (Vi-Rail, SIMPACK) [4,5].

Two specific reference systems have to be introduced in order to simplify the wheel and rail profiles description and, consequently, the model's equations: the auxiliary reference system and the local reference system. The auxiliary system $O_r x_r y_r z_r$ moves along the track centerline, following the wheelset during the dynamical simulations; the x_r axis is tangent to the center line of the track in the origin, O_r, whose position is defined so that the $y_r z_r$ plane contains the center of mass $\mathbf{G}_w$ of the wheelset, and the z_r axis is perpendicular to the plane of the track. The local system $O_w x_w y_w z_w$ is fixed on the wheelset, except for the rotation around its axis, and the x_w axis is parallel to the $x_r y_r$ plane (see Fig. 5(*b*)). In the following, for the sake of simplicity, the variables referred to the local system will be marked with the apex w, while those referred to the auxiliary system with the apex r; the variables belonging to the wheel and to the rail will be indicated with the subscripts w and r, respectively.

3.2.1 The Distance Method Algorithm. In this subsection, the algorithm used for detecting the contact points will be described. The main innovative aspect of the algorithm is the reduction of the original multidimensional contact problem (4D) to a simple scalar problem (1D), which can be easily handled by means of numerical methods with remarkable advantages:

- The multiple solution management is simpler
- A wide range of algorithms, even the elementary noniterative ones, can efficiently resolve the numerical problem
- The convergence can be easily achieved and the algorithm converges to the solutions with fewer iterations and less computational effort

The distance method algorithm (see Fig. 5(*a*)) starts from a classical formulation of the contact problem in multibody field; considering the adopted reference systems, the following geometrical conditions hold:

- The normal unitary vector relative to the rail surface $\mathbf{n}^r_r(\mathbf{P}^r_r)$ and the wheel surface unitary vector $\mathbf{n}^r_w(\mathbf{P}^r_w)$ have to be parallel (R^r_w is the rotation matrix that links the local system to the auxiliary one),

$$\mathbf{n}^r_r \times \mathbf{n}^r_w(\mathbf{P}^r_w) = \mathbf{n}^r_r(\mathbf{P}^r_r) \times R^r_w \mathbf{n}^w_w(\mathbf{P}^w_w) = 0 \qquad (1)$$

  The wheel and rail surfaces can be locally considered as revolution and extrusion surface, respectively: $\mathbf{P}^{wT}_w = (x_w,\, y_w,\, -\sqrt{w(y_w)^2 - x_w^2})$, $\mathbf{P}^{rT}_r = (x_r,\, y_r,\, r(y_r))$, where the generative function $w(y_w)$ and $r(y_r)$ are supposed to be known.
- The rail surface normal unitary vector $\mathbf{n}^r_r(\mathbf{P}^r_r)$ has to be parallel to the distance vector $\mathbf{d}^r = \mathbf{P}^r_w(x_w, y_w) - \mathbf{P}^r_r(x_r, y_r)$ between the generic point of the wheel and of the rail,

$$\mathbf{n}^r_r(\mathbf{P}^r_r) \times \mathbf{d}^r = 0 \qquad (2)$$

Alternately, the problem can also be equivalently formulated, imposing that the distance vector $\mathbf{d}^r$ is perpendicular both to the

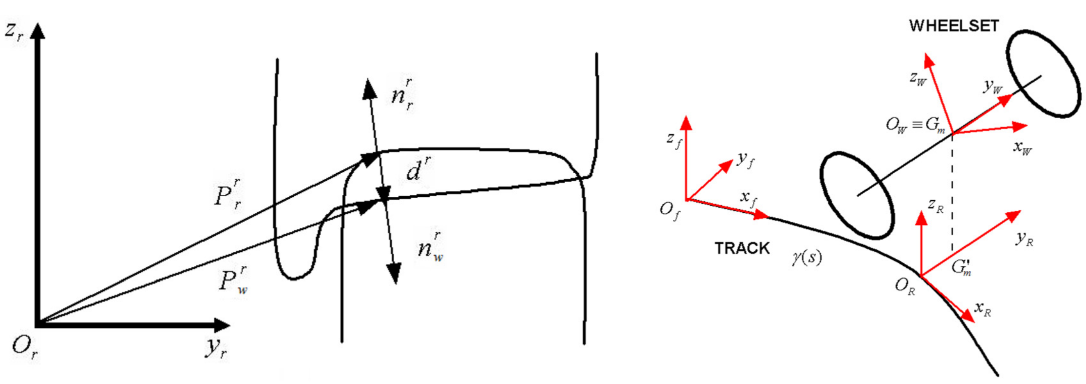

(a) (b)

Fig. 5 Distance method

wheel and to the rail tangent planes (respectively, $\pi_w(P^r_r)$ and $\pi_r(P^r_w)$). Nevertheless, due to the particular structure of the algebraic equations, the calculation and the resolution algorithm are more complicated than the ones arising from Eqs. (1) and (2).

The distance between the generic points on the wheel and on the rail can be expressed as

$$\mathbf{d}^r(x_w, y_w, x_r, y_r) = \mathbf{O}^r_w + R^r_w \mathbf{P}^w_w(x_w, y_w) + \mathbf{P}^r_r(x_r, y_r) \tag{3}$$

Thus, it depends on the four parameters (x_w, y_w, x_r, y_r) that identify a point on both the surfaces. The Eqs. (1) and (2) constitute a system with six scalar equations and four unknowns (x_w, y_w, x_r, y_r) (only four of the equations are independent). As stated previously, the 4D problem can be reduced to a scalar equation in the unknown y_w, expressing x_w, x_r, and y_r as functions of y_w. The second component of Eq. (1) leads to the following equation:

$$r_{13}\sqrt{w(y_w)^2 - x_w^2} = r_{11}x_w - r_{12}w(y_w)w'(y_w) \tag{4}$$

where r_{ij} are the elements of the R^r_w matrix. Calling $A = r_{13}$, $B = w(y_w)$, $C = r_{11}$, and $D = r_{12}w(y_w)w'(y_w)$, the previous equation becomes

$$A\sqrt{B^2 - x_w^2} = Cx_w - D \tag{5}$$

Hence, removing the radical and solving for x_W,

$$x_{w1,2}(y_w) = \frac{CD \pm \sqrt{C^2D^2 - (A^2 + C^2)(D^2 - A^2B^2)}}{A^2 + C^2} \tag{6}$$

As can be seen, there are two possible values of x_w for each y_w.

From the first component of Eq. (1), the following relation for $r'(y_r)$ holds:

$$r'(y_r)_{1,2} = \frac{r_{21}x_{r1,2}(y_w) - r_{22}w(y_w)w'(y_w) - r_{23}\sqrt{w(y_w)^2 - x_{w1,2}(y_w)^2}}{r_{32}w(y_w)w'(y_w) + r_{33}\sqrt{w(y_w)^2 - x_{w1,2}(y_w)^2}} \tag{7}$$

If $r'(y_r)_{1,2}$ is a decreasing monotonous function (considering separately the sides of the track), Eq. (7) is numerically invertible and a single pair, $y_{r1,2}(y_w)$, exists for each y_w value; otherwise, the numerical inversion is still possible, but will produce a further multiplication of the solution number.

By the second component of Eq. (2), the expression of $x_{r1,2}(y_w)$ can be obtained,

$$x_{r1,2}(y_w) = r_{11}x_{w1,2}(y_w) + r_{12}y_w - r_{13}\sqrt{w(y_w)^2 - x_{w1,2}(y_w)^2} \tag{8}$$

Finally, replacing the variables $x_{w1,2}(y_w)$, $x_{r1,2}(y_w)$, and $y_{r1,2}(y_w)$ in the first component of Eq. (2), the following 1D scalar equation can be written:

$$\begin{aligned} F_{1,2}(y_w) = & -r'\Big(G_{wz} + r_{32}y_w - r_{33}\sqrt{w^2 - x_{w1,2}{}^2} - b\Big) \\ & + -\Big(G_{wy} + r_{21}x_{w1,2} + r_{22}y_w \\ & - r_{23}\sqrt{w^2 - x_{w1,2}{}^2} - y_{r1,2}\Big) = 0 \end{aligned} \tag{9}$$

where G_{wx}, G_{wy}, and G_{wz} are the coordinates of the wheelset center of mass $\mathbf{G}^r_w$ in the auxiliary system. The expression in Eq. (9) consists of two scalar equations in the variable y_w easy to resolve numerically with the advantages previously mentioned. Thus, once obtained, the generic solution (indicated with the subscript i) y_{wi} of Eq. (9), the values of the unknowns $(x_{wi}, y_{wi}, x_{ri}$, and $y_{ri})$, and consequently the contact points $\mathbf{P}^r_{wi} = \mathbf{P}^r_w(x_{wi}, y_{wi})$ and $\mathbf{P}^r_{ri} = \mathbf{P}^r_r(x_{ri}, y_{ri})$ can be found by substitution.

Since the Eqs. (1) and (2) contain irrational terms, the generic solution $(x_{wi}, y_{wi}, x_{ri}$, and $y_{ri})$ must satisfy the following analytical conditions:

- The solution must be real
- The solution does not have to generate complex terms (that could be caused by the radicals in the equations)
- (x_{w1i}, y_{w1i}) and (x_{w2i}, y_{w2i}) must be effective solutions of Eq. (4) (check necessary because of the radical removal by squaring)

The following physical conditions have also to be respected, so that the contact is physically possible:

- The penetration between the wheel and rail surfaces ($\tilde{p}_n = \mathbf{d}^r \cdot \mathbf{n}^r_r$) have to be less or equal to zero, according to the adopted nomenclature
- Multiple solutions have to be rejected
- The normal curvatures of the wheel and rail surfaces in the longitudinal and lateral direction $(k_{1,wi}, k_{1,ri}, k_{2,wi}, k_{2,ri})$, evaluated in the contact points, have to satisfy the convexity condition in order to make the contact physically possible $(k_{1,wi} + k_{1,ri} > 0;\ k_{2,wi} + k_{2,ri} > 0)$.

3.2.2 The Contact Forces. The calculation of the contact forces for each contact point is based on a semielastic approach, which uses both Hertz's and Kalker's global theories (see Fig. 6).

The normal forces N^r (expressed in the auxiliary system) are calculated by means of Hertz's theory [6],

$$N^r = \left[-k_h|\tilde{p}_n|^\gamma + k_v|v_n|\,\frac{\mathrm{sign}(v_n) - 1}{2}\right]\frac{\mathrm{sign}(\tilde{p}_n) - 1}{2} \tag{10}$$

where:

- $\tilde{p}_n$ is the normal penetration previously defined
- γ is the Hertz's exponent equal to 3/2
- k_v is the contact damping constant ($k_v = \ 10^5$Ns/m)
- $v_n = \mathbf{V} \cdot \mathbf{n}^r_r$ is the normal penetration velocity ($\mathbf{V}$ is the velocity of the contact point $\mathbf{P}^r_w$ rigidly connected to the wheelset)
- k_h is the Hertzian constant and function both of the material properties and of the geometry of the contact bodies (curvatures and semiaxes of the contact patch) [6]

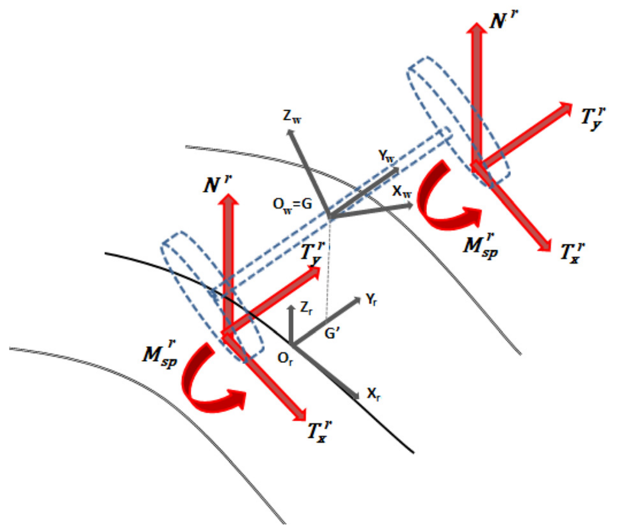

Fig. 6 Global forces acting at wheel and rail interface

The global creepages, ε (longitudinal ε_x, lateral ε_y, and spin creepage ε_{sp}), are calculated as follows:

$$\varepsilon_x = \frac{\mathbf{V}\cdot i_r}{\left\|\dot{\mathbf{G}}^r_w\right\|}, \quad \varepsilon_y = \frac{\mathbf{V}\cdot t^r_r\left(\mathbf{P}^r_r\right)}{\left\|\dot{\mathbf{G}}^r_w\right\|}, \quad \varepsilon_{sp} = \frac{\omega^r_w\cdot \mathbf{n}^r_r\left(\mathbf{P}^r_r\right)}{\left\|\dot{\mathbf{G}}^r_w\right\|} \tag{11}$$

where $\mathbf{V}$ is the velocity of contact point, $\mathbf{P}^r_w$, rigidly connected to the wheelset, $\dot{\mathbf{G}}^r_w$ is the wheelset center of mass velocity (taken as the reference velocity for the calculation of the global creepages), ω^r_w is the angular velocity of the wheelset expressed in the auxiliary system, $\mathbf{i}_r$ is the unit vector in the longitudinal direction of the auxiliary system, and $\mathbf{t}^r_r$ is the tangential unit vector to the rail profile.

The tangential contact forces $\tilde{\mathbf{T}} = \left(\tilde{T}^r_x\,,\ \tilde{T}^r_y\right)$ and the spin torque M^r_{sp} (expressed in the auxiliary system) are calculated by means of the Kalker's global theory,

$$\tilde{T}^r_x = -f_{11}\varepsilon_x, \quad \tilde{T}^r_y = -f_{22}\varepsilon_y - f_{23}\varepsilon_{sp} \tag{12}$$

$$M^r_{sp} = f_{23}\varepsilon_y - f_{33}\varepsilon_{sp} \tag{13}$$

where the coefficients f_{ij} are functions both of the materials and of the semiaxes of the contact patch,

$$f_{11} = abGC_{11}, \qquad f_{22} = abGC_{22}$$
$$f_{23} = (ab)^{3/2}GC_{23}, \quad f_{33} = (ab)^2GC_{33} \tag{14}$$

in which G is the wheel and rail combined shear modulus and C_{ij} are the Kalker's coefficients that can be found tabulated in literature [6].

Since the Kalker's theory is linear, to include the effect of the adhesion limit due to friction, a saturation criterion has to be introduced in the model to limit the magnitude of the tangential contact force, $\tilde{T}^r = \sqrt{\tilde{T}^{r2}_x + \tilde{T}^{r2}_y}$, which cannot exceed the slip value, $\mu_c N^r$ (μ_c is the kinematic friction coefficient). Therefore, a saturation coefficient ε_{sat} is defined as follows [10,11]:

$$\varepsilon_{\text{sat}} = \begin{cases} \dfrac{\mu_c N^r}{\tilde{T}^r}\left[\left(\dfrac{\tilde{T}^r}{\mu_c N^r}\right) - \dfrac{1}{3}\left(\dfrac{\tilde{T}^r}{\mu_c N^r}\right)^2 + \dfrac{1}{27}\left(\dfrac{\tilde{T}^r}{\mu_c N^r}\right)^3\right], & \text{if } \tilde{T}^r \le 3\mu_c N^r \\ \dfrac{\mu_c N^r}{\tilde{T}^r}, & \text{if } \tilde{T}^r > 3\mu_c N^r \end{cases} \tag{15}$$

In this way, the saturated tangential force will be $\mathbf{T}^r = \varepsilon_{\text{sat}}\tilde{\mathbf{T}}^r$.

4 The Wear Model

In this section, the three phases of the wear model will be described in detail: the local contact model, the evaluation of the amount of removed material due to wear, and the wheel and rail profile update.

4.1 The Local Contact Model.

The purpose of the local contact model is the calculation of the local contact variables into the contact patch (normal and tangential contact pressures p_n, p_t, and local creep s), starting from the corresponding global variables (contact points $\mathbf{P}^r_w$ and $\mathbf{P}^r_r$; contact forces N^r, T^r_x, and T^r_y; global creepage ε; and semiaxes of the contact patch a and b).

This model is based on the Kalker's local theory in the simplified version implemented in the algorithm FASTSIM; this algorithm contains an extremely efficient version (although necessarily approximate) of the Kalker theory commonly used in a railway field [6].

For the local analysis, a new reference system is defined at the wheel-rail interface on the contact plane (i.e., the common tangent plane between the wheel and rail surfaces). The x and y axes are the longitudinal and the transversal direction of the contact plane, respectively (see Figs. 7 and 9); therefore, they are not parallel to either the local reference system of the wheelset or the auxiliary system. The working hypothesis on which the algorithm is developed is the proportionality between the tangential contact pressure $\mathbf{p}_t$ and the elastic displacements $\mathbf{u}$ in a generic point of the contact patch,

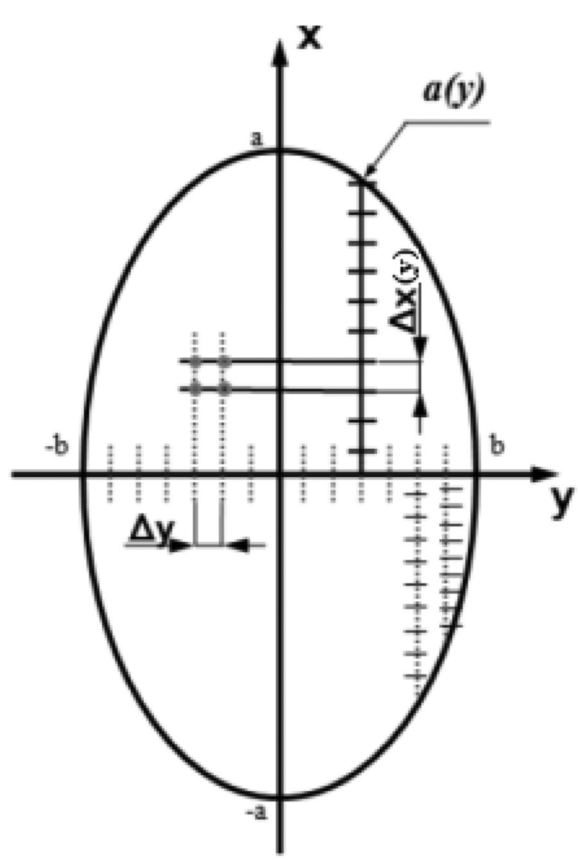

Fig. 7 Contact patch discretization

$$\mathbf{u}(x,\,y) = L\mathbf{p}_t(x,\,y), \quad L = L(\varepsilon,\,a,\,b,\,G,\,\nu) \tag{16}$$

where the flexibility L (function of the global creepages, ε, the semiaxes of the contact patch, a and b, the wheel and rail combined shear modulus, G, and the wheel and rail combined Poisson's ratio, ν) can be calculated as follows:

$$L = \frac{|\varepsilon_x|L_1 + |\varepsilon_y|L_2 + c|\varepsilon_{sp}|L_3}{\left(\varepsilon_x^2 + \varepsilon_y^2 + c^2\varepsilon_{sp}^2\right)^{1/2}} \tag{17}$$

with $L_1 = 8a/(3GC_{11})$, $L_2 = 8a/(3GC_{22})$, $L_3 = \pi a^2/(4GcC_{23})$, and $c = \sqrt{ab}$ (the constants, C_{ij}, and functions both of the Poisson's ratio, ν, and of the ratio, a/b, are the Kalker's parameters and can be found in literature).

The local creepages $\mathbf{s}$ can be calculated, deriving the elastic displacements and considering the rigid global creepages ($V = \left\|\dot{\mathbf{G}}^r_w\right\|$ is the vehicle speed),

$$\mathbf{s}(x,\,y) = \dot{\mathbf{u}}(x,\,y) + V\begin{pmatrix}\varepsilon_x \\ \varepsilon_y\end{pmatrix} \tag{18}$$

At this point, it is necessary to discretize the elliptical contact patch in a grid of points in which the quantities p_n, $\mathbf{p}_t$, and $\mathbf{s}$ will be evaluated. Initially, the transversal axis (in respect to the motion direction) of the contact ellipse has been divided in $n_y - 1$

equal parts of magnitude $\Delta y = 2b/(n_y - 1)$ by means of n_y equidistant nodes. Then, the longitudinal sections of the patch (long $2a(y) = 2a\sqrt{1 - y/b^2}$) have been divided in $n_x - 1$ equal parts of magnitude $\Delta x(y) = 2a(y)/(n_x - 1)$ by means of $\mathbf{n}_x$ equidistant nodes (see Fig. 7). This choice leads to a longitudinal resolution that is not constant and increases nearby the lateral edges of the ellipse, where the length $a(y)$ is shorter. This procedure provides more accurate results near the edges of the ellipse, where a constant resolution grid would generate excessive numerical noise. The values of the n_x and n_y parameters have to assure the right balance between precision and computational load; good values of compromise are in the range 25–50. AQ1

Once the contact patch is discretized, the FASTSIM algorithm allows the iterative evaluation both of the contact pressures value p_n and $\mathbf{p}_t$ and of the local creepage $\mathbf{s}$ in order to divide the contact patch in the adhesion and slip zone. Indicating the generic point of the grid with (x_i, y_j), $1 \le i \le n_x$, and $1 \le j \le n_y$, the normal contact pressure can be expressed as

$$p_n(x_i, y_j) = \frac{3}{2}\frac{N^r}{\pi ab}\sqrt{1 - \frac{x_i^2}{a^2} - \frac{y_j^2}{b^2}} \tag{19}$$

where N^r is the normal contact force, while the limit adhesion pressure $\mathbf{p}_A$ is

$$\mathbf{p}_A(x_i, y_j) = \mathbf{p}_t(x_{i-1}, y_j) - \begin{pmatrix} \varepsilon_x \\ \varepsilon_y \end{pmatrix} \frac{\Delta x(y_j)}{L} \tag{20}$$

Thus, knowing the variable values in the point (x_{i-1}, y_j), it is possible to pass to the point (x_i, y_j) as follows:

$$\text{if } \left\|\mathbf{p}_A(x_i, y_j)\right\| \le \mu p_n(x_i, y_j)$$
$$\Downarrow$$
$$\begin{cases} \mathbf{p}_t(x_i, y_j) = \mathbf{p}_A(x_i, y_j) \\ \mathbf{s}(x_i, y_j) = 0 \end{cases} \tag{21a}$$

$$\text{if } \left\|\mathbf{p}_A(x_i, y_j)\right\| > \mu p_n(x_i, y_j)$$
$$\Downarrow$$
$$\begin{cases} \mathbf{p}_t(x_i, y_j) = \mu p_n(x_i, y_j)\mathbf{p}_A(x_i, y_j)/\left\|\mathbf{p}_A(x_i, y_j)\right\| \\ \mathbf{s}(x_i, y_j) = \dfrac{LV}{\Delta x(y_j)}\left(\mathbf{p}_t(x_i, y_j) - \mathbf{p}_A(x_i, y_j)\right) \end{cases} \tag{21b}$$

where μ is the static friction coefficient; Eqs. (21) and (22) hold, respectively, in the adhesion and slip zone.

Iterating the procedure for $2 \le i \le n_x$ and successively for $1 \le j \le n_y$ and assuming as boundary conditions $\mathbf{p}_t(x_1, y_j) = 0$ and $\mathbf{s}(x_1, y_j) = 0$ for $1 \le j \le n_y$ (i.e., pressures and creepages zero out of the contact patch), the desired distribution of $p_n(x_i, y_j)$, $\mathbf{p}_t(x_i, y_j)$, and $\mathbf{s}(x_i, y_j)$ can be determined.

4.2 The Wear Evaluation.

4.2 The Wear Evaluation. The following working hypotheses have been considered to evaluate the distribution of removed material on wheel and rail, in agreement with Trenitalia and RFI requests:

- The outputs of the wear model are the mean wheel and rail profiles to be used in the next step, which include the effect of the wear on all the wheels of the considered vehicle and on all the N_c curves of the statistical analysis
- dry conditions in the wheel-rail interface

The calculation of the wear is based on an experimental relationship between the volume of removed material by wear and the frictional work at the contact interface [3,8]; particularly, the used relationship is able to directly evaluate the specific volumes of removed material $\delta_{P_{wi}^{jk}(t)}(x, y)$ and $\delta_{P_{ri}^{jk}(t)}(x, y)$ related to the i-th contact points $P_{wi}^{jk}(t)$ and $P_{ri}^{jk}(t)$ on the j-th wheel and rail pair during the k-th of the N_c dynamic simulations.

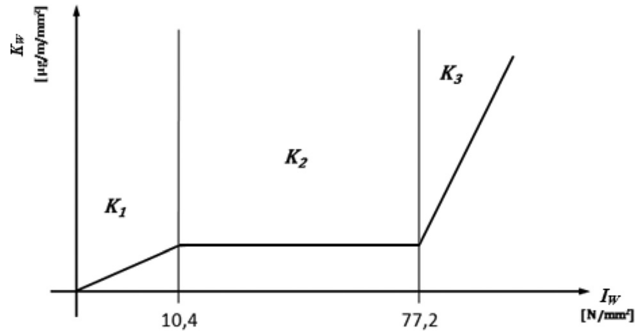

Fig. 8 Trend of the *wear rate* K_W

The calculation of $\delta_{P_i^{jk}(t)}(x, y)$ requires, first of all, the evaluation of the friction power developed by the tangential contact stresses; to this aim, the *wear index* I_W (expressed in $\mathrm{N/mm^2}$) is defined as follows:

$$I_W = \frac{\mathbf{p}_t \cdot s}{V} \tag{22}$$

This index is experimentally correlated with the *wear rate* K_W (expressed in $\mu\mathrm{g/(m \cdot mm^2)}$), which represents the mass of removed material for unit of distance traveled by the vehicle (expressed in m) and for the unit of surface (expressed in $\mathrm{mm^2}$). Wear tests carried out in the case of metal-metal contact with dry surfaces using a twin disc test machine can be found in literature [3]. The experimental relationship between K_W and I_W adopted for the wear model described in this work is the following (see Fig. 8):

$$K_W(I_W) = \begin{cases} 5.3 * I_W & I_W < 10.4 \\ 55.12 & 10.4 \le I_W \le 77.2 \\ 61.9 * I_W - 4723.56 & I_W > 77.2 \end{cases} \tag{23}$$

After the evaluation of the *wear rate* $K_W(I_W)$ (the same both for the wheel and for the rail), the specific volume of removed material on the wheel and on the rail (for unit of distance traveled by the vehicle and for unit of surface) can be calculated as follows (expressed in $\mathrm{mm^3/(m \cdot mm^2)}$):

$$\delta_{P_{wi}^{jk}(t)}(x, y) = K_W(I_W)\frac{1}{\rho} \tag{24}$$

$$\delta_{P_{ri}^{jk}(t)}(x, y) = K_W(I_W)\frac{1}{\rho} \tag{25}$$

where ρ is the material density (expressed in $\mathrm{kg/m^3}$).

4.3 Profile Update. The profile update strategy is the set of numerical procedures that allows the calculation of the new profiles of wheel $w_n(y_w)$ and rail $r_n(y_r)$ (i.e., the profiles at the next step), starting from the old profiles of wheel $w_o(y_w)$ and rail $r_o(y_r)$ (i.e., the profiles at the current step) and all the distributions of removed material $\delta_{P_{wi}^{jk}(t)}(x, y)$ and $\delta_{P_{ri}^{jk}(t)}(x, y)$. The update strategy, besides evaluating the new profiles, is necessary for additional reasons:

(1) the necessity to remove the numerical noise that characterizes the distributions $\delta_{P_i^{jk}(t)}(x, y)$ and that, due to non-physical alterations of the new profiles, can cause problems to the global contact model
(2) the need to mediate the distributions $\delta_{P_i^{jk}(t)}(x, y)$ in order to obtain a single profile both for the wheel (that includes the

wear effects of all the wheels of the considered vehicle) and the rail (that includes the effects of all the N_c curves) as output of the wear model

The following main steps can be distinguished:

- *Longitudinal integration*:

$$\frac{1}{2\pi w(y_{wi}^{jk})}\int_{-a(y)}^{+a(y)} \delta_{P_{wi}^{jk}(t)}(x,y)dx = \delta_{P_{wi}^{jk}(t)}^{\text{tot}}(y) \quad (26)$$

$$\frac{1}{l_{\text{track}}}\int_{-a(y)}^{+a(y)} \delta_{P_{ri}^{jk}(t)}(x,y)dx = \delta_{P_{ri}^{jk}(t)}^{\text{tot}}(y) \quad (27)$$

This operation sums all the wear contributions in the longitudinal direction and spreads the wheel wear along the circumference of radius $w(y_{wi}^{jk})$ and the rail wear along the length l_{track} of the curved tracks on which the results of the vehicle dynamics are calculated, so to obtain the mean value of removed material for each considered contact point (expressed in $\text{mm}^3/(\text{m}\cdot\text{mm}^2)$). The difference between the terms $1/l_{\text{track}}$ and $1/2\pi w(y_{wi}^{jk})$ (the track length is much greater than the wheel circumference length) is the main cause that leads the wheel to wear much faster than the rail and, consequently, to a different scale of magnitude of the two investigated phenomena (according to the physical phenomena in which the rail has a life much greater in respect to the wheel).

For this reason, as will be better explained in the following, it is necessary to develop a different strategy for the update of the wheel and rail profile, respectively. In this research, the following strategies have been adopted:

(1) For the wheel update, the total mileage km_{tot} traveled by vehicle (derived from the experimental data provided by Trenitalia and RFI) is subdivided into constant steps of length equal to km_{step}

(2) For the rail update, the vehicle number N_{tot} corresponding to the tonnage burden on the track [12] is subdivided into constant steps equal to N_{step}

- *Time integration*

$$\int_{T_{in}}^{T_{end}} \delta_{P_{wi}^{jk}(t)}^{\text{tot}}(y)V(t)dt \approx \int_{T_{in}}^{T_{end}} \delta_{P_{wi}^{jk}(t)}^{\text{tot}}(s_w - s_{wi}^{cjk}(t))V(t)dt = \Delta_{P_{wi}^{jk}}(s_w) \quad (28)$$

$$\int_{T_{in}}^{T_{end}} \delta_{P_{ri}^{jk}(t)}^{\text{tot}}(y)V(t)dt \approx \int_{T_{in}}^{T_{end}} \delta_{P_{ri}^{jk}(t)}^{\text{tot}}(s_r - s_{ri}^{cjk}(t))V(t)dt = \Delta_{P_{ri}^{jk}}(s_r) \quad (29)$$

The time integration sums all the wear contributes coming from the dynamical simulation to obtain the depth of removed material for wheel $\Delta_{P_{wi}^{jk}}(s_w)$ and rail $\Delta_{P_{ri}^{jk}}(s_r)$ expressed in $\text{mm} = \text{mm}^3/\text{mm}^2$. In order to have a better accuracy in the calculation of the worn profiles, the natural abscissas s_w and s_r of the curves $w(y_w)$ and $r(y_r)$ have been introduced. In particular, the following relations locally hold (see Fig. 9):

$$y \approx s_w - s_{wi}^{cjk}(t) \quad y \approx s_r - s_{ri}^{cjk}(t) \quad (30)$$

$$w(y_w) = w(y_w(s_w)) = \tilde{w}(s_w) \quad r(y_r) = r(y_r(s_r)) = \tilde{r}(s_r) \quad (31)$$

AQ2 where the natural abscissas of the contact points s_{wi}^{cjk} and s_{wi}^{cjk} can be evaluated from their positions P_{wi}^{jk} and P_{ri}^{jk}.

- *Sum on the contact points*

$$\sum_{i=1}^{N_{\text{PDC}}} \Delta_{P_{wi}^{jk}}(s_w) = \Delta_{jk}^{w}(s_w) \quad (32)$$

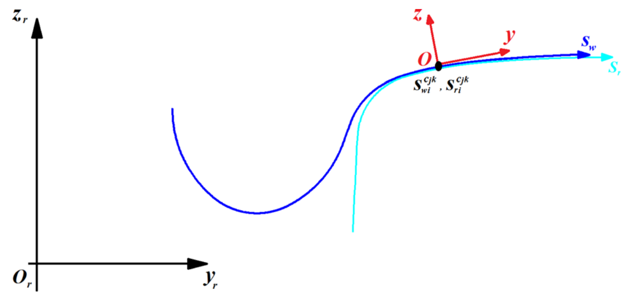

Fig. 9 Natural abscissa for the wheel and rail profile

$$\sum_{i=1}^{N_{\text{PDC}}} \Delta_{P_{ri}^{jk}}(s_r) = \Delta_{jk}^{r}(s_r) \quad (33)$$

where N_{PDC} is the maximum number of contact points of each single wheel (and, respectively, of each single rail). The contact patches are usually less than N_P and their number can vary during the simulation; hence, since the summation is extended to N_P, the contribution of the missing points has been automatically set equal to zero.

- *Average on the vehicle wheels and on the dynamical simulations*

$$\sum_{k=1}^{N_c} p_k \frac{1}{N_w}\sum_{j=1}^{N_w} \Delta_{jk}^{w}(s_w) = \overline{\Delta}^{w}(s_w) \quad (34)$$

$$\sum_{k=1}^{N_c} p_k \frac{1}{N_w}\sum_{j=1}^{N_w} \Delta_{jk}^{r}(s_r) = \overline{\Delta}^{r}(s_r) \quad (35)$$

where N_w is the number of vehicle wheels, while the p_k, $1 \le k \le N_c$, and $\sum_{k=1}^{N_C} p_k = 1$ are the normalized weights related to the N_C simulations of the statistical analysis and needed to differentiate the relative impact on the wear of each curve. The average on the number of wheel-rail pairs has to be evaluated in order to obtain, as output of the wear model, a single average profile both for the wheels of the considered vehicle and for the rails of the curves of the statistical analysis.

- *Scaling*

The aim of the scaling procedure is to amplify the small quantity of material removed relative to the overall mileage traveled by the vehicle during the N_C simulations; that is, $km_{\text{prove}} = l_{\text{track}}$. In fact, the necessity of acceptable computational time for the multibody simulations leads us to adopt a small value of the km_{prove} length. AQ3

The chance to take advantage of the scaling lies in the *almost linearity* of the wear model with respect to the traveled distance (obviously only inside the discrete step km_{step}).

In this work, a constant discrete step km_{step} has been chosen to update the wheel and rail profiles (see Fig. 10 and Eqs. (36) and (37)). This approach requires limited computational load without losing accuracy if compared with different suitable strategies as the adaptive step (due to the almost linearity of the wear model inside the discrete step km_{step}) [8].

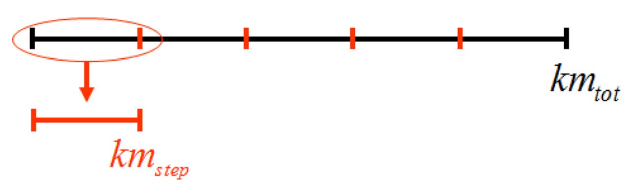

Fig. 10 Discretization of the total mileage

The evaluation of the discrete step and the consequent scaling of $\overline{\Delta}^{w}(s_w)$ and $\overline{\Delta}^{r}(s_r)$ represent the major difference between wheel update and rail update,

(1) The removed material on the wheel due to wear is proportional to the distance traveled by the vehicle; in fact, the wheel is frequently in contact with the rail in a number of times proportional to the distance. If the real chosen mileage, km_{tot}, that the vehicle has to run is divided in discrete steps of length, km_{step} (km_{tot} can be chosen, depending on the purpose of the simulations; for example, equal to the re-profiling intervals) (see Fig. 10), the material removed on the wheel has to be scaled according to the following law:

$$\overline{\Delta}^{w}(s_w)\frac{km_{\mathrm{step}}}{km_{\mathrm{prove}}} = \overline{\Delta}^{wsc}(s_w) \tag{36}$$

After the scaling, the quantity $\overline{\Delta}^{wsc}(s_w)$ is related to a spatial step with a length equal to km_{step}, instead of km_{prove}. The choice of the spatial step must be a good compromise between numerical efficiency and the accuracy required by the wear model. A km_{step} too small compared to km_{tot} would provide accurate results, but excessive calculation times; the contrary happens with km_{step} too big if compared to km_{tot}.

(2) The depth of rail wear does not depend on the distance traveled by the vehicle; in fact, the rail tends to wear out only in the zone where it is crossed by the vehicle, and, increasing the traveled distance, the depth of removed material remains the same. On the other hand, the rail wear is proportional to the total tonnage M_{tot} burden on the rail and, thus, to the total vehicle number, N_{tot}, moving on the track. Therefore, if N_{step} is the vehicle number moving in a discrete step, the quantity of rail removed material at each step will be

$$\overline{\Delta}^{r}(s_r) * N_{\mathrm{step}} = \overline{\Delta}^{rsc}(s_r) \tag{37}$$

where N_{step} is calculated, subdividing in constant step the vehicle number N_{tot} corresponding to the total tonnage that has to be simulated; N_{tot} can be obtained starting from the vehicle mass M_v: $N_{\mathrm{tot}} = M_{\mathrm{tot}}/M_v$.

- *Smoothing of the removed material*

$$\Im\left[\overline{\Delta}^{wsc}(s_w)\right] = \overline{\Delta}^{wsc}_{sm}(s_w) \tag{38}$$

$$\Im\left[\overline{\Delta}^{rsc}(s_r)\right] = \overline{\Delta}^{rsc}_{sm}(s_r) \tag{39}$$

The smoothing of the removed material function is necessary both to remove the numerical noise and the physically meaningless short spatial wavelengths that affect this quantity (that would be passed to the new profiles $\tilde{w}_n(s_w)$ and $\tilde{r}_n(s_r)$ of wheel and rail causing problems to the global contact model). To this end, a discrete filter (i.e., a moving average filter with window size equal to 1%–5% of the total number of points in which the profiles are discretized) has been used. This solution is simple, and at the same time, the filter does not change the total mass of removed material, as obviously required.

- *Profile update*

$$\begin{pmatrix} y_w(s_w) \\ \tilde{w}_o(s_w) \end{pmatrix} - \overline{\Delta}^{wsc}_{sm}(s_w)\mathbf{n}^{r}_{w} \xrightarrow{\text{re-parameterization}} \begin{pmatrix} y_w(s_w) \\ \tilde{w}_n(s_w) \end{pmatrix}$$
$$\begin{pmatrix} y_r(s_r) \\ \tilde{r}_o(s_r) \end{pmatrix} - \overline{\Delta}^{rsc}_{sm}(s_r)\mathbf{n}^{r}_{r} \xrightarrow{\text{re-parameterization}} \begin{pmatrix} y_r(s_r) \\ \tilde{r}_n(s_r) \end{pmatrix} \tag{40}$$

The last step consists of the update of the old profiles, $\tilde{w}_o(s) = w_o(y)$ and $\tilde{r}_o(s_r) = r_o(y_r)$, to obtain the new profiles, $\tilde{w}_n(s) = w_n(y)$ and $\tilde{r}_n(s_r) = r_n(y_r)$; since the removal of material occurs in the normal direction to the profiles ($\mathbf{n}^{r}_{w}$ and $\mathbf{n}^{r}_{r}$ are the outgoing unit vectors for the wheel and rail profiles, respectively), once removed, the quantities $\overline{\Delta}^{wsc}_{sm}(s_w)$ and $\overline{\Delta}^{rsc}_{sm}(s_r)$, a re-parameterization of the profiles is needed in order to obtain again curves parameterized by means of the curvilinear abscissa. AQ4

5 Wear Model Validation

In this section, the wear model validation will be presented. Initially, the set of N_c curvilinear tracks, on which the dynamic simulations of the *DMU Aln 501 Minuetto* vehicle have been performed, will be introduced; moreover, the wear control parameters for the wheel and rail will be defined (the flange height (FH), the flange thickness (FT), the flange steepness (QR), and the quota (QM) for the rail). Then, the experimental data measured on the Aosta-Pre Saint Didier track and their processing will be introduced. Finally, the simulation strategy used to analyze the wear both on the wheel and on the rail will be described, and the results obtained with the wear model will be analyzed and compared with the experimental data.

5.1 Statistical Analysis of the Aosta-Pre Saint Didier Track. Starting from the data of the whole Aosta-Pre Saint Didier track (provided by RFI), a statistical analysis has been performed by dividing the line both in radius classes (determined by $R_{\min}$ and $R_{\max}$) and in superelevation classes (determined by $h_{\min}$ and $h_{\max}$) [9]. More particularly, five superelevation subclasses are defined for each radius class. All the N_c curved tracks are shown in Table 3. Blank rows are present because, for certain classes, no curves were found.

The set consists of $N_c = 18$ distinct elements (17 real curves and the straight line) characterized by a radius value R_c, a superelevation value H, a traveling speed V, and a statistical weight p_k (with $1 \le k \le N_c$) that represents the frequency with which each curve appears on the considered railway track (Aosta-Pre Saint Didier line). The radii R_c are calculated by means of the weighted average on all the curve radii included in that subclass (the weighted factor is the length of the curves in the real track). For each subclass, the value H is the most frequent superelevation value among the values found in that subclass. The traveling speeds V are calculated, imposing a threshold value on the uncompensated acceleration $a^{\lim}_{nc} = 0.6\ \mathrm{m/s^2} : \tilde{V}^2/R_c - Hg/s = a^{\lim}_{nc}$ (s is the railway gauge and g is the gravity acceleration).

The estimated speed $\tilde{V}$ has been then compared with the maximum velocity $V_{\max}$ on the line to get the desired traveling speed $V = \min(\tilde{V}, V_{\max})$.

5.2 Wear Control Dimensions. The reference quotas FH, FT, and QR are introduced in order to estimate the wheel profile evolution due to the wear without necessarily knowing the whole profile shape (see Fig. 11). According to these quotas, the user will be able both to establish when the worn wheel profile will have to be re-profiled and to detect if the wear compromises the dynamical stability of the vehicle [13].

The procedure to define the reference quotas is the following:

(1) First of all, the point $P0$ is defined on the profile at 70 mm from the internal vertical face of the wheel
(2) Then, the point $P1$ is introduced on the profile 2 mm under the flange vertex
(3) Finally, the point $P2$ is determined on the profile 10 mm under the point $P0$
(4) The wear control parameters are then calculated as follows: the flange thickness FT is the horizontal distance between the internal vertical face and the point $P2$; the flange steepness QR is the horizontal distance between the points $P1$ and $P2$, while the flange height FH is the vertical distance

Table 3 Data of the curvilinear tracks of the statistical analysis

R_{min} (m)	R_{max} (m)	Superelevation h_{min}–h_{max} (mm)	R_c (m)	H (mm)	V (km/h)	p_k %
147.1	156.3	0	—	—	—	—
		10–40	—	—	—	—
		60–80	—	—	—	—
		90–120	150	120	55	0.77
		130–160	—	—	—	—
156.3	166.7	0	—	—	—	—
		10–40	—	—	—	—
		60–80	—	—	—	—
		90–120	160	110	55	0.48
		130–160	165	140	55	0.56
166.7	178.6	0	—	—	—	—
		10–40	—	—	—	—
		60–80	—	—	—	—
		90–120	170	110	55	0.82
		130–160	175	130	55	1.55
178.6	192.3	0	—	—	—	—
		10–40	—	—	—	—
		60–80	—	—	—	—
		90–120	190	100	55	8.37
		130–160	180	130	55	0.45
192.3	208.3	0	—	—	—	—
		10–40	—	—	—	—
		60–80	—	—	—	—
		90–120	200	90	55	20.64
		130–160	200	130	60	4.00
208.3	227.3	0	—	—	—	—
		10–40	—	—	—	—
		60–80	220	80	55	0.70
		90–120	220	100	55	3.76
		130–160	—	—	—	—
227.3	250.0	0	—	—	—	—
		10–40	—	—	—	—
		60–80	240	80	55	7.26
		90–120	240	110	60	5.28
		130–160	—	—	—	—
250.0	312.5	0	—	—	—	—
		10–40	—	—	—	—
		60–80	270	70	55	3.91
		90–120	270	90	60	5.29
		130–160	—	—	—	—
312.5	416.7	0	—	—	—	—
		10–40	—	—	—	—
		60–80	370	60	55	2.26
		90–120	345	100	70	1.63
		130–160	—	—	—	—
416.7	∞	0	∞	0	70	32.27

between $P0$ and the flange vertex (all the distances are considered positive).

An additional control parameter is then introduced to evaluate the evolution of the rail wear. Particularly, the QM quota is defined as the rail head height in the point $y_r = 760$ mm with respect to the center line; this y_r value depends on the railway gauge (equal to 1435 mm in the Aosta-Pre Saint Didier line) and on the laying angle α_p of the track (equal to 1/20 rad). Physically, the QM quota gives information on the rail head wear (see Fig. 12).

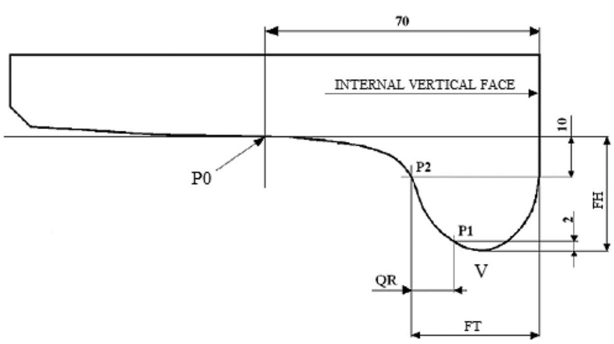

Fig. 11 Definition of the wheel wear control parameters

5.3 Experimental Data and Their Processing.

The experimental data provided by Trenitalia and RFI are related only to the

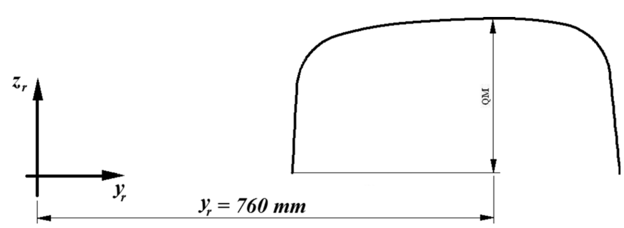

Fig. 12 Definition of rail wear control parameter

Table 4 Experimental data of the *Aln 501 Minuetto* DM061

km	Quotas	1r	1l	2r	2l	3r	3l	4r	4l	5r	5l	6r	6l	7r	7l	8r	8l
		Wheel diameter 816 mm		Wheel diameter 815 mm		Wheel diameter 824 mm		Wheel diameter 823 mm		Wheel diameter 823 mm		Wheel diameter 823 mm		Wheel diameter 819 mm		Wheel diameter 820 mm	
0	FT	30.953	30.944	30.983	30.784	31.099	30.957	30.938	31.076	30.401	30.367	30.830	30.987	30.437	30.717	30.852	30.933
	FH	27.970	27.894	28.141	28.043	27.969	28.187	28.030	28.271	28.245	27.918	28.141	27.982	28.013	27.937	28.333	27.883
	QR	10.208	10.140	10.424	10.457	10.220	10.306	10.279	10.833	10.332	10.445	10.364	10.219	10.421	10.500	10.338	10.396
1426	FT	29.855	28.977	30.283	29.317	30.118	29.383	30.152	29.450	29.796	29.799	30.288	29.483	29.802	29.085	30.267	29.316
	FH	28.010	27.923	28.104	28.108	28.000	28.249	28.095	28.278	28.248	28.284	28.247	28.030	28.997	28.003	30.383	27.919
	QR	9.297	8.226	9.822	8.956	9.344	8.749	9.551	9.072	9.635	9.767	9.773	8.763	9.593	8.883	9.675	8.762
2001	FT	29.056	28.498	29.722	28.878	29.441	28.667	29.629	28.717	29.153	28.101	29.739	28.841	29.066	28.447	29.625	28.777
	FH	27.990	27.880	28.161	28.080	29.998	28.248	28.128	28.283	28.290	27.994	28.273	28.022	28.027	28.014	28.362	27.957
	QR	8.404	7.558	9.233	8.637	8.702	7.950	8.873	8.436	9.144	8.141	9.235	8.086	9.038	8.152	9.248	8.373
2575	FT	28.259	27.096	29.333	28.045	28.972	28.385	29.029	28.124	29.053	27.600	29.095	28.505	28.553	27.866	29.205	28.473
	FH	28.009	27.089	28.173	28.020	28.063	28.243	28.090	28.241	28.285	27.963	28.244	28.085	28.030	28.018	28.352	27.968
	QR	7.198	7.024	8.853	8.163	8.123	7.598	8.438	7.791	8.868	7.395	8.559	7.840	8.372	7.340	8.777	7.900

wheel wear and consists of the evolutions of the reference dimensions measured on three different *DMUs Aln 501 Minuetto* (conventionally named DM061, DM068, and DM082) during the service on the Aosta-Pre Saint Didier line. As can be seen by example in Table 4 for the vehicle MD061, the reference quota values have been measured for all the vehicle wheels (each vehicle has eight wheelsets, as specified in Sec. 3.1). However, the following data processing has been necessary in order to compare the experimental data with the mean profile evaluated by the numerical simulation:

AQ5 AQ6

(1) Initially, the arithmetic mean on all the sixteen vehicle wheels, necessary to obtain a single wheel profile and to reduce the measurement errors affecting the experimental data, has been performed
(2) Then, a scaling of the quota values has been carried out to delete the offset on the initial value of the quotas; this procedure imposes that all the wear control parameters start from their nominal values (the standard values for the ORE S 1002 profile have been used) in order to remove the initial differences among the vehicles due to measurement errors
(3) The arithmetic mean on the three vehicle MD061, MD068, and MD082 has not been carried out, so to maintain a dispersion range for the experimental data

AQ7

The experimental data, properly processed, are summarized in Table 5. As can be seen, the flange height FH remains approximately constant, because of the low mileage traveled by the vehicles, while the flange thickness FT and the flange steepness QR decrease almost linearly and highlight, according to the sharpness of the track, the wear concentration in the wheel flange.

Table 5 Experimental data processed

Vehicle	Distance traveled (km)	FH (mm)	FT (mm)	QR (mm)
DM061	0	28.0	32.5	10.8
	1426	28.2	31.5	9.8
	2001	28.1	30.8	9.1
	2575	28.0	30.2	8.6
DM068	0	28.0	32.5	10.8
	1050	28.0	31.8	10.0
	2253	28.0	30.2	8.5
	2576	28.0	30.0	8.4
DM082	0	28.0	32.5	10.8
	852	28.0	32.3	10.6
	1800	28.0	31.3	9.6
	2802	28.0	30.3	8.7
	3537	27.6	30.0	8.3

5.4 Simulation Strategy. As explained in Sec. 4.3, the wear on wheel and rail evolves with different time scales (several orders of magnitude) and a full simulation of such events would require a too heavy computational effort. For this reason, the following specific algorithm has been adopted for updating the profiles:

(1) To have a good compromise between calculation times and result accuracy, both for the wheel and for the rail, five discrete steps have been chosen, $n_{sw} = 5$ and $n_{sr} = 5$:
   (a) The choice of the wheel km_{step} (see Sec. 4.3) has been made, considering the whole distance traveled available from experimental data, equal to $km_{\mathrm{tot}} \approx 3500$ km (see Table 5); thus, the single step length will be

$$km_{\mathrm{step}} = \frac{km_{\mathrm{tot}}}{n_{sw}} \approx 700 \text{ km} \tag{41}$$

   (b) To estimate the vehicle number, N_{tot} (see Sec. 4.3), a criterion found in literature and based on the total tonnage burden on the track has been used [12]. Particularly, a proportionality relationship between tonnage and wear holds: a rail wear of 1 mm on the rail head height every 100 Mt (millions of tons) of accumulated tonnage. In order to obtain an appreciable rail wear, a maximum value of removed material depth of 2 mm on the rail head height has been hypothesized (naturally, this value can be changed according to the requirements of the simulation). Starting from the vehicle mass M_v (see Table 1), the number of vehicles which should pass to reach the $M_{\mathrm{tot}} = 200$ Mt on the track has been calculated,

$$N_{\mathrm{tot}} = \frac{M_{\mathrm{tot}}}{M_v} \approx 2000000 \tag{42}$$

and then

$$N_{\mathrm{step}} = \frac{N_{\mathrm{tot}}}{n_{sr}} \approx 400000 \tag{43}$$

(2) The wear evolution on wheel and rail has been decoupled, because of the different scales of magnitude:
   (a) While the wheel wear evolves, the rail is supposed to be constant; in fact, in the considered time scale, the rail wear variation is negligible

(b) Because of the time scale characteristic of the rail wear, each discrete rail profile comes in contact, with the same frequency, with each possible wheel profile. Due to this reason, for each rail profile, the whole wheel wear evolution (from the original profile to the final profile) has been simulated.

Based on the two previous hypotheses, the simulations have been carried out according to the following strategy:

Wheel profile evolution (w_i^0) at first rail step (r_0)

$$p_{1,1}\{\ (w_0^0 \quad r_0) \rightarrow (w_1^0 \quad r_0) \rightarrow \ldots \rightarrow (w_4^0 \quad r_0) \rightarrow w_5^0$$

Average on the rails for the calculation of the second rail step (r_1)

$$p_{1,2}\left\{ \begin{pmatrix} w_0^0 & r_0 \\ w_1^0 & r_0 \\ \vdots & \vdots \\ w_4^0 & r_0 \end{pmatrix} \rightarrow \begin{pmatrix} r_1^{(1)} \\ r_1^{(2)} \\ \vdots \\ r_1^{(5)} \end{pmatrix} \rightarrow r_1 \right.$$

$\vdots$

Wheel profile evolution (w_i^4) at fourth rail step (r_4)

$$p_{5,1}\{\ (w_0^4 \quad r_4) \rightarrow (w_1^4 \quad r_4) \rightarrow \ldots \rightarrow (w_4^4 \quad r_4) \rightarrow w_5^4$$

Average on the rails for the calculation of the fifth rail step (r_5)

$$p_{5,2}\left\{ \begin{pmatrix} w_0^4 & r_4 \\ w_1^4 & r_4 \\ \vdots & \vdots \\ w_4^4 & r_4 \end{pmatrix} \rightarrow \begin{pmatrix} r_5^{(1)} \\ r_5^{(2)} \\ \vdots \\ r_5^{(5)} \end{pmatrix} \rightarrow r_5 \right. \tag{44}$$

where w_i^j indicates the i-th step of the wheel profile that evolves on the j-th step of the rail profile r_j. The initial profiles w_0^j are always the same for each j and correspond to the unworn wheel profile (ORE S 1002).

Initially, the wheel (starting from the unworn profile w_0^0) evolves on the unworn rail profile r_0 in order to produce the discrete wheel profiles $w_1^0, w_2^0, \ldots, w_{nsw}^0$ (step $p_{1,1}$). Then, the virtual rail profiles $r_1^{(i+1)}$, obtained by means of the simulations (w_i^0, r_0) with $0 \le i \le n_{sw} - 1$, are arithmetically averaged so as to get the updated rail profile r_1 (step $p_{1,2}$). This procedure can be repeated n_{sr} times in order to perform all the rail discrete steps (up to the step $p_{5,2}$).

The computational effort required by the simulation strategy is the following:

(a) In the wheel wear study (steps $p_{j+1,1}$ with $0 \le j \le n_{sr} - 1$), for each update of the rail profile r_j, the whole wheel wear loop w_i^j with $0 \le \ i \le \ n_{sw} - 1$ (n_{sw} steps of simulation) is simulated. The computational effort results of $n_{sw} \times n_{sr} = 25$ steps both for the dynamical analysis (in SIMPACK) and for the wear model are necessary to calculate the removed material on the wheel (in MATLAB). So the total number of simulation steps is $2(n_{sw} \times n_{sr}) = 50$.

(b) In the rail wear study (steps $p_{j+1,2}$ with $0 \le \ j \le \ n_{sr} - 1$), the dynamical analyses are the same of the previous case, because for each rail step, the wheel profiles w_i^j $(0 \le i \le n_{sw} - 1)$ are simulated on r_j in order to obtain $r_j^{(i+1)}$ and, thus, the updated rail profile r_{j+1} by means of an arithmetic average. Therefore, no additional dynamical analyses are needed. In this case, only the wear model steps must be simulated, so as to get the removed material on the rail. Consequently, the total number of simulation steps is $n_{sw} \times n_{sr} = 25$.

Table 6 Computational time

	Mean computational time			
	UNIFI model		SIMPACK model	
Processor	Dynamical simulation	Wear simulation	Dynamical simulation	Wear simulation
INTEL Xeon CPU E 5430 2.66 GHz 8 GB RAM	2h 2′	31′	2h 58′	38′

The characteristics of the processor used in the simulations and the mean computational times relative to each discrete step of the model loop (dynamical simulation and wear simulation) are briefly summarized in Table 6. In this research activity, a preliminary study has been performed comparing the numerical efficiency of the developed model with a reliable benchmark wear model present within the SIMPACK multibody software. The comparison showed a reduction of the calculation time both as regards the dynamical simulations (due to the high efficiency of the global contact model [4,5] and the use of user routine directly implemented in C/C++ environment) and as regards the wear model (thanks to the MATLAB CS-functions that allow the direct compilation of the Matlab code in C/C++) (see Table 6).

5.5 Evolution of Wear Control Dimensions. In this section, the evolution of the wheel reference quotas numerically evaluated by means of the wear model (flange thickness FT, flange height FH, and flange steepness QR) will be compared with the experimental data concerning the three *DMUs Aln 501 Minuetto* vehicles. Furthermore, the rail reference quota QM evolution will be shown and compared with the criterion present in literature based on the total tonnage burden on the track [12].

The progress of FT dimension for the n_{sr} discrete steps of the rail is shown in Fig. 13; as it can be seen, the decrease of the dimension is almost linear with the traveled distance, except in the first phases, where the profiles are still not conformal enough. The FH quota progress is represented in Fig. 14 and shows that, due to the presence of many sharp curves in the statistical analysis of the track and to the few kilometers traveled, the wheel wear is mainly localized on the flange rather than on the tread and the flange height remains near constant, in agreement with experimental data. The QR trend is shown in Fig. 15; also, the flange steepness decreases almost linearly, leading to an increase of the conicity of the flange. Finally, the evolution of the wheel control parameters remains quantitatively and qualitatively similar as the rail wear raises.

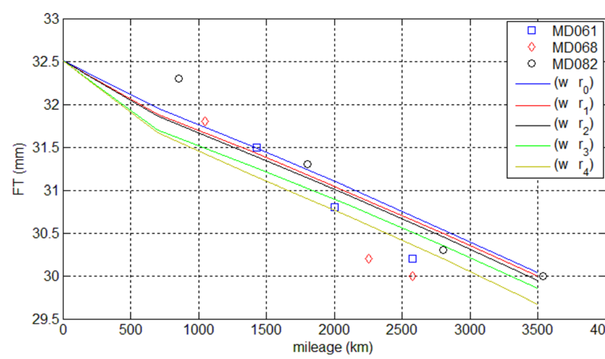

Fig. 13 FT dimension progress

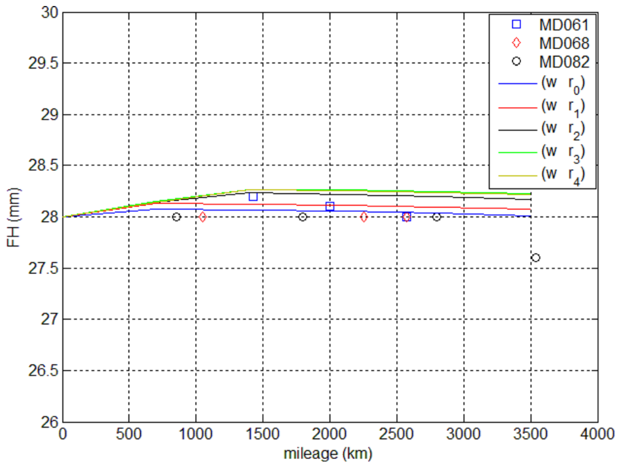

Fig. 14 FH dimension progress

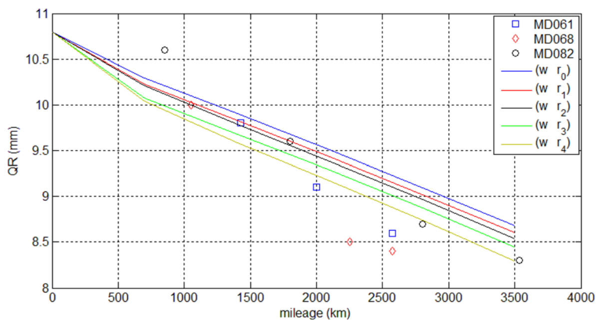

Fig. 15 QR dimension progress

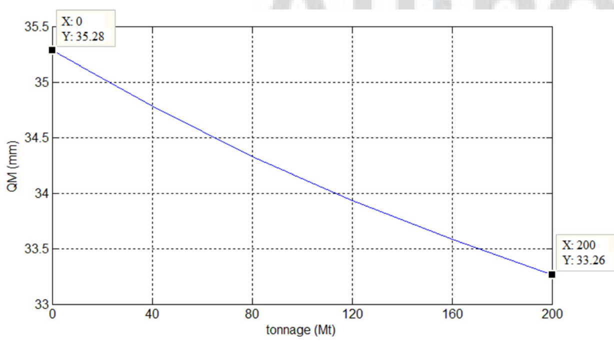

Fig. 16 QM dimension progress

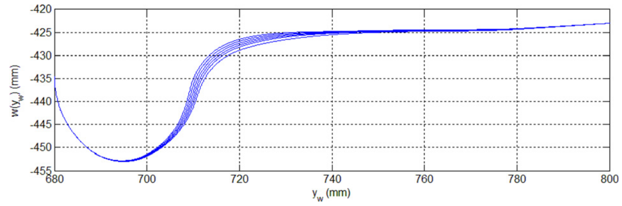

Fig. 17 Evolution of the wheel profile on the r_0 rail

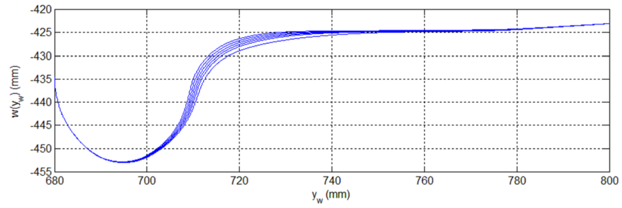

Fig. 18 Evolution of the wheel profile on the r_1 rail

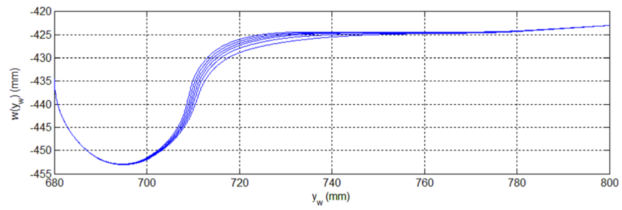

Fig. 19 Evolution of the wheel profile on the r_2 rail

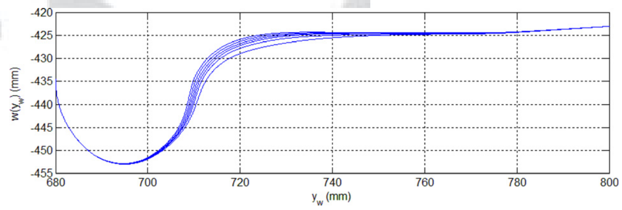

Fig. 20 Evolution of the wheel profile on the r_3 rail

Although the simulated mileage is quite short, considering the mean traveled distance between two turnings of the wheels in a standard scenery (in fact, the FH quota remains almost constant), the variations of the FT and QR dimensions are remarkable and it highlights the wear problems affecting this vehicle in traveling this railway line. In conclusion, the comparisons show that the outputs of the wear model are consistent with the experimental data, both for the flange dimension (FH, FT) and for the conicity (QR); the slightly steeper development of the experimental data than the simulation can be explained with the dispersion of the experimental data and with the wear mechanisms, like plastic and pitting wear, not considered in the developed wear model.

Finally, the QM evolution for the analysis of the rail wear is presented in Fig. 16 and shows the almost linear dependence between the rail wear and the total tonnage burden on the track; the amount of removed material on the rail profile is in agreement with the criterion present in literature (1 mm on the rail head height every 100 Mt of accumulated tonnage).

5.6 Evolution of the Wheel and Rail Profiles. The wear evolution on the wheel profiles evolving on each rail r_j (with $0 \leq j \leq n_{sr-1}$ and $n_{sr} = 5$) is reported in Figs. 17–21. As previously stated, the wheel profile evolution is described by means of $n_{sw} = 5$ steps and the spatial step km_{step} has been chosen equal to 700 km, since the total mileage km_{tot} is 3500 km.

The quite limited distance traveled by the vehicle justifies the low wear on the wheel tread and entails a small reduction of the rolling radius. However, the high tortuosity of the considered track leads to appreciable wear on the wheel flange. In Fig. 17, focusing on the flange zone, the higher wear rate during the first steps can be observed because of the initial nonconformal contact that characterizes the coupling between the ORE S 1002 wheel profile and the UIC 60 rail profile with an inclination of $\alpha_p = 1/20$ rad; then, the rate decreases, becoming more regular and constant in the last steps, when the contact is more and more conformal.

Also, as regards the wheel profile evolution (as for the reference quotas), the trend remains quantitatively and qualitatively the same as the rail wear raises (see Figs. 18–21).

In Fig. 22, the evolution of the rail profile, described by means of $n_{sr} = 5$ discrete steps and with N_{step} equal to 400 000 (the vehicle number N_{tot}, corresponding to the total studied tonnage M_{tot}, is 2 000 000) is shown. The value of total tonnage taken into account ($M_{\text{tot}} = 200$ Mt) causes an appreciable wear on the rail head,

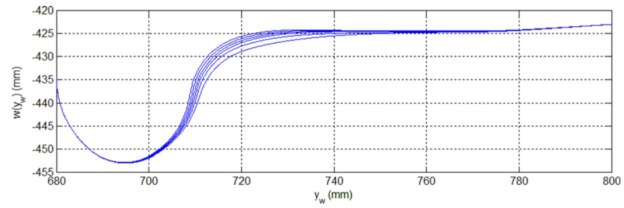

Fig. 21 Evolution of the wheel profile on the r_4 rail

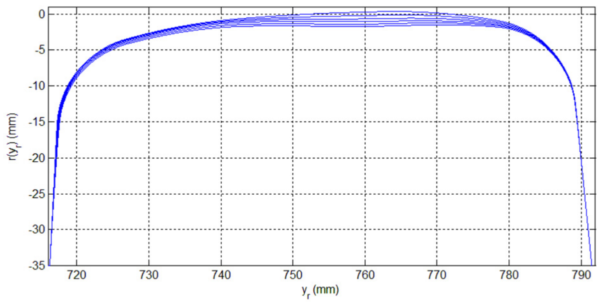

Fig. 22 Evolution of the rail profile

while it is not sufficient to produce a high wear also on the rail shoulder.

6 Conclusions

In this work, the authors presented a complete model for the wheel and rail wear prediction in railway application, developed thanks to the collaboration with Trenitalia S.p.A and Rete Ferroviaria Italiana (RFI), which provided the necessary technical and experimental data for the model validation. The whole model is made up of two parts, which mutually interact. The first one evaluates the vehicle dynamics and comprises both the multibody model of the vehicle implemented in Simpack Rail and a global wheel-rail contact model (developed by the authors in previous works) for the calculation of the contact points and of the contact forces. The second one is the wear model, which, starting from the outputs of the multibody simulations, evaluates the amount of material to be removed by wear. The interaction between the two parts is not a continuous time process, but occurs at discrete steps; consequently, the evolution of the wheel and rail geometry is described through several intermediate profiles. The developed model reproduces quite well the evolution of all the profile characteristic dimensions describing the wear progress on both the wheel and the rail.

Future developments will be based on further experimental data provided by Trenitalia and RFI, referring both to railway tracks with an higher mileage than the Aosta-Pre Saint Didier line and to advanced wear on the wheel (especially on the tread) and on the rail. A new analysis will be then carried out in order to further validate the whole model by means of the experimental data and of the comparison with other wear models present within commercial multibody software, like SIMPACK. Finally, the design of wheel profiles optimized from the wear viewpoint will be performed according to the research interest of Trenitalia.

Acknowledgment

The authors would like to thank Engg. R. Cheli and G. Grande of Trenitalia S.p.A. for providing and giving the permission to edit the data both of the vehicle *DMU Aln 501 Minuetto* and of the wheel wear evolution; a special thanks also goes to the Engg. R. Mele and M. Finocchi of Rete Ferroviaria Italiana for the Aosta-Pre Saint Didier line data. AQ8

References

[1] Pearce, T. G., and Sherratt, N. D., 1991, "Prediction of Wheel Profile Wear," Wear, **144**, pp. 343–351.
[2] Pombo, J., Ambrosio, J., Pereira, M., Lewis, R., Dwyer-Joyce, R., Ariaudo, C., and Kuka, N., 2010, "A Study on Wear Evaluation of Railway Wheels Based on Multibody Dynamics and Wear Computation," Multibody Syst. Dyn., **24**, pp. 347–366.
[3] Braghin, F., Lewis, R., Dwyer-Joyce, R. S., and Bruni, S., 2006, "A Mathematical Model to Predict Railway Wheel Profile Evolution Due to Wear," Wear, **261**, pp. 1253–1264.
[4] Meli, E., Falomi, S., Malvezzi, M., and Rindi, A., 2008, "Determination of Wheel-Rail Contact Points With Semianalytic Methods," Multibody Syst. Dyn., **20**, pp. 327–358.
[5] Auciello, J., Meli, E., Falomi, S., and Malvezzi, M., 2009, "Dynamic Simulation of Railway Vehicles: Wheel/Rail Contact Analysis," Veh. Syst. Dyn., **47**, pp. 867–899.
[6] Kalker, J. J., 1990, *Three-Dimensional Elastic Bodies in Rolling Contact*, Kluwer Academic, Dordrecht, Netherlands.
[7] Bozzone, M., Pennistri, E., and Salvini, P., 2010, "A Lookup Table-Based Method for Wheel-Rail Contact Analysis," J. Multibody Dyn., **225**, pp. 127–138. AQ10
[8] Enblom, R., and Berg, M., 2005, "Simulation of Railway Wheel Profile Development Due to Wear Influence of Disc Braking and Contact Environment," Wear, **258**, pp. 1055–1063.
[9] Toni, P., 2010, "Ottimizzazione dei Profili Delle Ruote su Binario con Posa 1/20," Trenitalia S.p.A. Technical Report.
[10] Shabana, A. A., Tobaa, M., Sugiyama, H., and Zaazaa, K. E., 2005, "On the Computer Formulations of the Wheel/Rail Contact Problem," Nonlinear Dyn., **40**, pp. 169–193.
[11] Iwnicki, S., 2003, "Simulation of Wheel-Rail Contact Forces," Fatigue Fract. Eng. Mater. Struct., **26**, pp. 887–900.
[12] Esveld, C., 1985, *Modern Railway Track*, Delft University of Technology, Delft, Netherland, 2001. AQ9
[13] 2010, "Railway Applications - In Service Wheelset Operation Requirements - In Service and Off Vehicle Wheelset Maintenance," Report No. EN 15313.